

LWT Based Robust Color Image Watermarking Using QR Factorization and DCT

Omar Moftah Abodena
Electrical & electronic engineering
dept.
Faculty of engineering
University of Gharyan
Gharyan, Libya
omar.abodena@gu.edu.ly

Abstract—This paper proposes a novel robust blind color image watermarking technique that combines entropy analysis, lifting wavelet transform (LWT), QR factorization, and discrete cosine transform (DCT) for copyright protection. The RGB components of the color image are first separated, and the R component is then subjected to the 2-level LWT. Following DCT is applied to the 2-level LWT's high-frequency sub-band, the DCT coefficients are separated into 4x4 non-overlapping blocks. Each chosen block is then subjected to QR factorization, and the watermark is embedded in the first row and first column element of the upper triangular matrix. Numerous simulated tests show that the presented scheme is highly imperceptible and robust to attacks. The presented watermarking scheme performs better than the others in terms of invisibility, according to comparisons with comparable schemes.

Keywords—QR factorization, security, watermarking, entropy analysis, lifting wavelet transform, discrete cosine transform

I. INTRODUCTION

With the availability of widespread alter tools for digital form, several issues have occurred like forgery of digital contents, modification, and tampering. Therefore, digital data integrity and copyright protection content have increased and become important security issues. The digital watermarking technique represents an important technique in the protection of digital form [1]. The classifications of watermarking techniques based on the nature of watermark information can be fragile watermarking, semi-fragile watermarking, and robust watermarking [2]. In the fragile watermarking technique, the watermark information cannot be extracted after making small alterations to the watermark. On the other side, the robust watermarking technique can resist image processing and geometrical attacks. Therefore, the semi-fragile watermarking technique can maintain a good balance between fragility and robustness [3]. Basically, the two aspects that are dependent on the quality of the digital watermarking scheme are: imperceptibility and robustness. Visual distortion can occur by the modification of the original image, however, fewer modifications can lead to a good image quality [4]. Over the last decade, to improve the quality of digital watermarking and the ability to withstand watermarking attacks, several techniques have been presented [5-7] which can be classified into two domains: spatial and frequency domains inclusive lifting wavelet transform [8-10], Fourier transform [11-13], discrete cosine transform [14-16], and matrix decomposition [17-25].

One of the research problems is how to implement a robust watermarking scheme that achieves high imperceptibility, large capacity, high security, and strong robustness to common attacks. This paper proposes a blind color image watermarking scheme for copyright protection that depends on discrete cosine transform and QR factorization, combined with lifting wavelet transform and entropy analysis to address that problem.

The contributions of this presented work include three aspects:

- The combination of DCT, LWT, and QR factorization is used to obtain the benefits of these transformations for improving invisibility and the ability to withstand watermarking attacks such as energy compaction characteristics provided by DCT, several elements that can be used to hide the watermark providing by QR factorization, and excellent frequency localization properties providing by LWT.
- For enhancing the security of the presented method, a pseudo-random sequence is used.
- For achieving a better trade-off between imperceptibility and robustness, the entropy analysis is used.

The categorization of this paper is as follows. Section II introduces discrete cosine transform, lifting wavelet transform, entropy analysis QR factorization, and random permutation function. Section III introduces the watermark embedding process and the watermark extraction process. Section IV provides the experimental results and discussions. The conclusions of this paper are summarized in Section V.

II. PRELIMINARIES CONCEPTS

A. Lifting wavelet transform

Let $\{s_i[m]\}_{m \in \mathbb{Z}}$ [26] be a signal whose level of resolution is $i \in M \cup \{0\}$. A 2π periodic function of a signal $\{s_i[m]\}_{m \in \mathbb{Z}}$ is defined as follows:

$$S_i(w) = \sum_{m \in \mathbb{Z}} s_i[m] e^{-jwm}, w \in R \quad (1)$$

a signal $\{s_i[m]\}_{m \in \mathbb{Z}}$ which its polyphase representation is shown as follows:

$$S_i(w) = S_{e,i}(2w) + S_{o,i}(2w) e^{-jwm} \quad (2)$$

where the polyphase decomposition of a signal $\{s_i[m]\}_{m \in \mathbb{Z}}$ is given by

$$S_{e,i}(w) = \sum_{m \in Z} s_i[2m]e^{-jwm}, S_{o,i}(w) = \sum_{m \in Z} s_i[2m + 1]e^{-jwm} \quad (3)$$

The polyphase components' representation of the signal are given by components $S_{e,i}(w)$ and $S_{o,i}(w)$.

The lifting wavelet transform deals with the effective management of individual polyphase components. The LWT is completely compatible with both the frequency and time domains and can be defined in both. The LWT's technique in the frequency domain is equivalent to factorizing a polyphase matrix made up of Laurent polynomials' polyphase components.

The following four steps can be used to realize the LWT: **Step 1 (split):** A signal is divided into an odd-indexed component $\{s_{o,i-1}[m]\}_{m \in Z}$ and an even-indexed component $\{s_{e,i-1}[m]\}_{m \in Z}$ which is called split sequences. These two split sequences, which correlate to polyphase components are dealt with by the LWT, $\{s_{e,i-1}[m]\}_{m \in Z}$ and $\{s_{o,i-1}[m]\}_{m \in Z}$ which correspond to polyphase components $S_{e,i}(w)$ and $S_{o,i}(w)$.

$$s_{e,i-1}[m] = s_i[2m], s_{o,i-1}[m] = s_i[2m + 1] \quad (4)$$

Step 2 (predict): The predictor \mathcal{P} that acts on the even-indexed sequence $\{s_{e,i-1}[m]\}_{m \in Z}$ predicts the odd-indexed sequence $\{s_{o,i-1}[m]\}_{m \in Z}$.

$$d_{i-1}[m] = s_{o,i-1}[m] - (\mathcal{P} s_{e,i-1})[m] \quad (5)$$

Here, the operator \mathcal{P} represents the lifting operator.

Step 3 (update): The updater u that updates the even-indexed sequence $\{s_{e,i-1}[m]\}_{m \in Z}$ operates on the odd indexed sequence $\{d_{i-1}[m]\}_{m \in Z}$ which is predicted using the predictor \mathcal{P} .

$$s_{i-1}[m] = s_{e,i-1}[m] - (u d_{i-1})[m] \quad (6)$$

Step 4 (scaling): The results can be measured for a certain normalization in this step.

$$s_{i-1}[m] = Ks_{i-1}[m], d_{i-1}[m] = 1/K d_{i-1}[m], K \in R \quad (7)$$

B. Discrete cosine transform

One technique for converting a picture into the frequency domain is the discrete cosine transform, which has the benefits of high performance, precision, and energy concentration. DCT has therefore been used extensively in image-processing applications. The carrier picture is first separated into 8×8 sub-blocks, and DCT is then applied to each block to enhance the DCT transform performance. Three frequency subbands are included in the DCT results: high, middle, and low frequencies. Watermarks alter images because low-frequency coefficients contain significant perceptual information. The watermarked image becomes susceptible to low-pass filtering when high-frequency coefficients are embedded because they contain detailed information. Consequently, it is common practice to incorporate the watermark using the middle-frequency DCT

block coefficients [27]. Eq. (8) defines the 2D-DCT of a $M \times M$ picture $F(x, y)$ as follows:

$$F(u, v) = a(u)a(v) \times \left[\sum_{x=0}^{M-1} \sum_{y=0}^{M-1} f(x, y) \times \cos \frac{(2x+1)u\pi}{2M} \cos \frac{(2y+1)v\pi}{2M} \right] \quad (8)$$

where

$$a(u) = \begin{cases} \sqrt{1/M}, & u = 0 \\ \sqrt{2/M}, & u = 1, 2, \dots, M - 1 \end{cases} \quad (9)$$

x and y are the spatial domain coordinates, u and v are the frequency domain coordinates, $F(u, v)$ is the frequency coefficient at the coordinate (u, v) , and (v) is comparable to (u) .

C. QR factorization

In computer science, engineering, and mathematics, QR factorization is widely utilized. In particular, QR is frequently used as a subroutine in quadratic programming, to solve linear least squares problems, determine the rank of matrices, solve severely ill-conditioned linear systems, and compute Eigenvalues [28]. A QR factorization takes a matrix $A \in R^{m \times n}$ and factors it into the product as follows:

$$A = QR \quad (10)$$

where R is upper triangular and Q is orthonormal.

D. Entropy analysis

The degree of unpredictability in the image can be measured by the entropy. Entropy lists the image's information content. It characterizes the degree of ambiguity or chance present in an image. An image's quality increases with the amount of information it contains. Entropy, often known as Shannon's entropy or entropy of information, is a concept used in information theory to quantify the degree of uncertainty in an information source. The formula for Shannon's entropy is [29]:

$$E(x) = - \sum p(x) \log p(x) \quad (11)$$

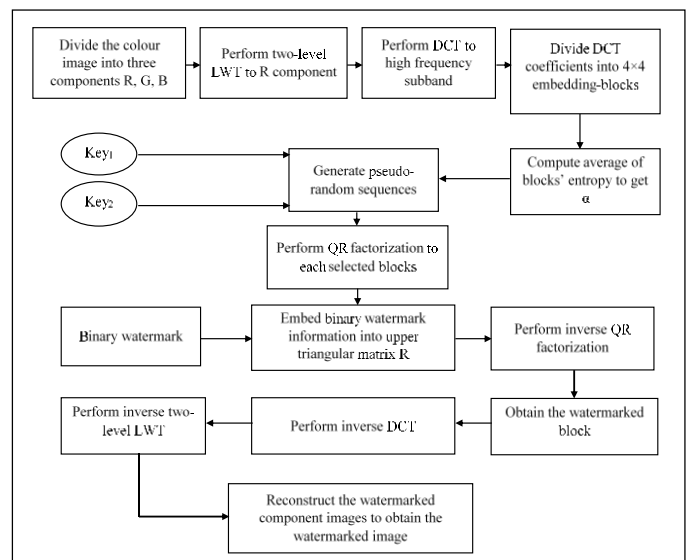


Fig. 1. The diagram of the watermark embedding process.

III. PROPOSED ALGORITHM

The proposed robust watermarking technique is divided into two processes, called; the watermark embedding and extraction processes which can be described in more detail as follows.

A. Watermark embedding

- 1) Divide the color image into RGB components.
- 2) Apply 2-level LWT to the R component and select the high_frequency subband of the 2-level where the R component is the best component for having high values in both imperceptibility and robustness.
- 3) Apply DCT high-frequency subband.
- 4) Divide DCT coefficients for obtaining 4×4 non-overlapping blocks which number of blocks is 64^2 .
- 5) Calculate the entropy of each block to obtain the average of entropy blocks as scaling factor α .
- 6) Generate the pseudo-random sequences utilizing randperm-function depending on key_1 and key_2 for having 2-random values.
- 7) Apply QR factorization for selecting 4×4 blocks depending on the pseudo-random sequences.
- 8) Modify the magnitudes M_1 and M_2 utilizing the binary watermark information w :

$$if\ w(i, j) = 1, \begin{cases} M_1 = 0.25\alpha \\ M_2 = -0.50\alpha \end{cases} \quad (12)$$

$$if\ w(i, j) = 0, \begin{cases} M_1 = -0.25\alpha \\ M_2 = 0.50\alpha \end{cases} \quad (13)$$

where $(1 \leq i, j \leq N)$, and α denotes the scaling factor.

- 9) Compute the potential quantization outcomes T_1 and T_2 utilizing the modified magnitudes M_1 and M_2 .

$$T_1 = 2k\alpha + M_1 \quad (14)$$

$$T_2 = 2k\alpha + M_2 \quad (15)$$

where $k = \text{floor}(\text{ceil}(r_{1,1}/\alpha)/2)$, $\text{floor}(\cdot)$ indicates the least nearest integer and $\text{ceil}(\cdot)$ indicates as the largest nearest integer.

- 10) Hide the binary watermark by selecting the first-column, first-row component $r_{1,1}$ of upper triangular matrix R as below:

$$d'_{1,1} = \begin{cases} T_2 & \text{if } \text{abs}(r_{1,1} - T_2) < \text{abs}(r_{1,1} - T_1) \\ T_1 & \text{else} \end{cases} \quad (16)$$

where $\text{abs}(\cdot)$ denotes the absolute value.

- 11) Replace the $r_{1,1}$ with $d'_{1,1}$ and after that apply the inverse QR factorization for obtaining the A' watermarked block.

$$A' = QR' \quad (17)$$

- 12) Repeat steps 7–11 for embedding bits of watermark.

- 13) Combine watermarked blocks.
- 14) Apply IDCT to combined watermarked blocks for obtaining the modified high-frequency subband.
- 15) Apply the inverse of the 2-level LWT utilizing the modified high-frequency subband to have the watermarked image.
- 16) Reconstruct the components of watermarked R, G, and B for having the watermarked color image.

The block diagram of the presented embedding process is given in Fig. 1.

B. Watermark extraction

- 1) Divide the watermarked color image into RGB components.
- 2) Apply 2-level LWT to the R component and select the high_frequency subband of the 2-level.
- 3) Apply DCT high-frequency subband.
- 4) Divide DCT coefficients for obtaining 4×4 non-overlapping blocks which number of blocks is 64^2 .
- 5) Calculate the entropy of each block to obtain the average of entropy blocks as scaling factor α .
- 6) Generate the pseudo-random sequences utilizing randperm-function depending on key_1 and key_2 for having 2-random values.
- 7) Apply QR factorization for selecting 4×4 blocks depending on the pseudo-random sequences.
- 8) Extract the binary watermark information utilizing the first-row, first-column component $r'_{1,1}$ of upper triangular matrix R as below:

$$w'_{i,j} = \text{mod}(\text{ceil}\left(\frac{r'_{1,1}}{\alpha}\right), 2) \quad (18)$$

where $(1 \leq i, j \leq N)$ and $\text{mod}(\cdot)$ indicates the modulo operation.

- 9) Repeat 7–8 for extracting bits of watermark.

The block diagram of the presented extraction process is given in Fig. 2.

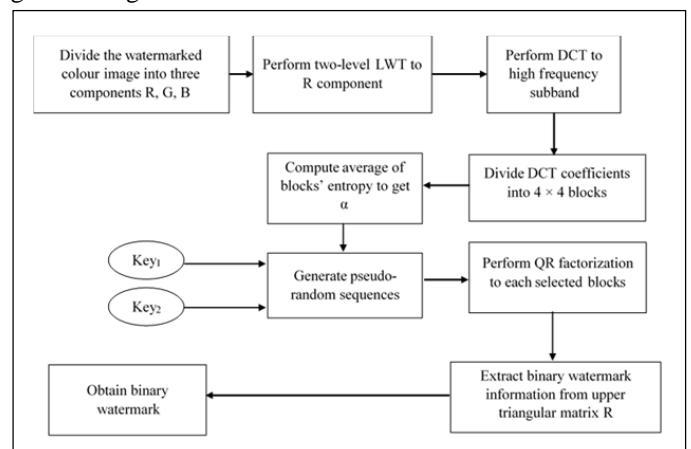


Fig. 2. The diagram of the watermark extraction process.

IV. RESULTS AND DISCUSSION

Due to obtaining experimental results, Five RGB common pinchmarket images (size = 1024 × 1024) are used which are from the USC-SIPI [30] database for presenting the results of this method to make a comparison of the method performance with existing techniques. The pinchmarket images are “Airplane”, “Baboon”, “Peppers”, “Sailboat”, and “Lena” which are shown in Fig. 3, whereas three watermarks (size = 64×64) are used as shown in Fig. 4. Invisibility measurement peak signal-to-noise ratio (PSNR) has been used to evaluate the quality between watermarked and original images while robustness measurement normalized cross-correlation (NC) has been used to evaluate the ability to withstand watermarking attacks [31].

A popular objective tool for evaluating the quality of watermarked images is PSNR, which computes the pixel difference between the original and the degraded image. The quality of the watermarked image and the watermarking technique can be both obtained with a greater PSNR value. The PSNR for color digital images is defined as follows [27]:

$$PSNR = 10 \log \frac{N_1 \times N_2 \times M \times 255^2}{\sum_{x=1}^{N_1} \sum_{y=1}^{N_2} \sum_{j=1}^M [I(x,y,j) - I^*(x,y,j)]^2} dB \quad (19)$$

$I(x,y,j)$ is the pixel value of the component j of the carrier image at the (x,y) location, $I^*(x,y,j)$ is the pixel value of the component j of the watermarked image at the (x,y) location, N_1 and N_2 are the number of rows and columns of the original carrier image, and M is the number of image components.

Furthermore, one objective measure for assessing the watermarking algorithm's robustness is normalized cross-correlation (NC). NC has a value between 0 and 1. The resemblance between the two images increases with the NC value. The following formula is used to get the NC value [27]:

$$NC = \frac{\sum_{j=1}^3 \sum_{x=1}^M \sum_{y=1}^N (W(x,y,j) \times W'(x,y,j))}{\sqrt{\sum_{j=1}^3 \sum_{x=1}^M \sum_{y=1}^N [W(x,y,j)]^2} \sqrt{\sum_{j=1}^3 \sum_{x=1}^M \sum_{y=1}^N [W'(x,y,j)]^2}} \quad (20)$$

W for the original color digital watermark image, W' stands for the extracted color digital watermark image, M and N for the watermark image's size, and j for the index of the color image's component parts.

Several types of attacks employed for obtaining the image experimental results are given below.

- Cropping: Removing watermarked images from the top 50% of the collection.
- Scaling: Making the watermarked images 5 times larger.
- Poisson noise: Including Poisson noise in the watermarked images.
- Blurring: Applying a blurring value of 0.5 to the watermarked images.
- Gamma correction: The watermarked images are subjected to a 1.0 gamma adjustment.
- Sharpening: Using a 0.5 quantity value to sharpen the watermarked images.

- Flipping: Turning the watermarked images from top to bottom.
- JPEG 2000 compression: Using the JPEG 2000 compression with a 1 compression ratio to perform watermarked images.
- Median filter: The watermarked images with a 2 × 1 window size are subjected to the median filter where the median value in the 2-by-1 region surrounding each output pixel in the watermarked image is contained.

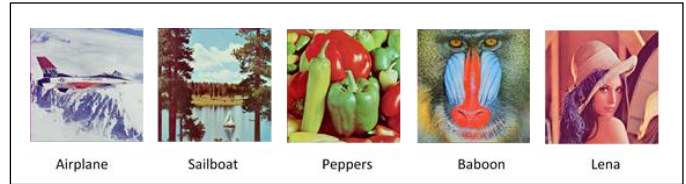


Fig. 3. The color host images.

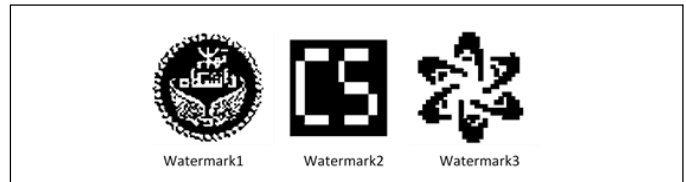


Fig. 4. The images of the watermark.

TABLE I. THE PSNR VALUES UNDER NO_ATTACKS

Host Image	Watermark1	Watermark2	Watermark3
Airplane	55.320	55.298	55.308
Sailboat	50.653	50.650	50.644
Peppers	51.628	51.632	51.623
Baboon	47.394	47.386	47.389
Lena	54.694	54.685	54.687

TABLE II. THE NC VALUES UNDER NO_ATTACKS

Host Image	Watermark1	Watermark2	Watermark3
Airplane	1.000	1.000	1.000
Sailboat	0.999	1.000	0.998
Peppers	1.000	1.000	1.000
Baboon	1.000	0.999	0.999
Lena	1.000	1.000	1.000

The PSNR and NC values of the watermarked images under no attacks are shown in Tables I and II. In general, high PSNR values show that the presented scheme performs better in terms of invisibility, while high NC values show that the presented scheme performs better in terms of robustness. While the average NC value is 1.000, the average PSNR value is 51.933 dB.

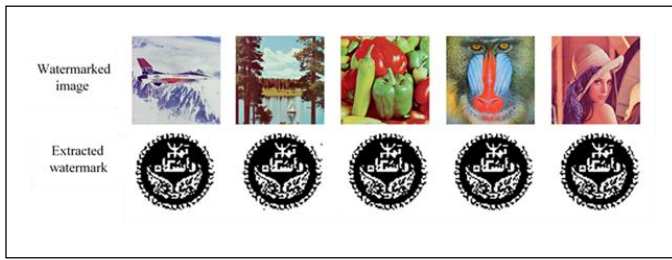


Fig. 5. The watermarked images and extracted watermark_1 under no_attack.



Fig. 6. The watermarked images and extracted watermark_2 under no_attack.

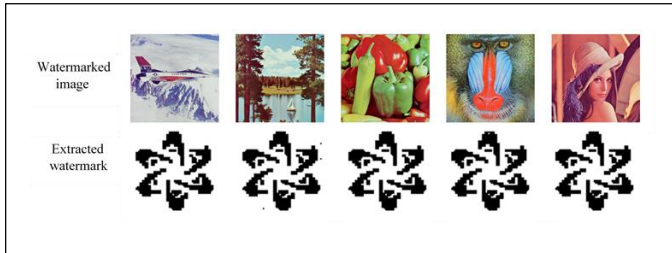


Fig. 7. The watermarked images and extracted watermark_3 under no_attack.

Figures 5 and 7 in the visual observations display the watermarked images with various watermark images that are under no attack. Table II and figures 5 to 7 demonstrate that the watermark images can be fully extracted and resemble the original watermark images, indicating that the presented scheme is more resistant to frequent attacks. Additionally, as seen in figures 5 to 7 and tables I to II, the watermarked and original images are more alike, indicating that the presented scheme is more imperceptible.

Figures 8 to 10 show the extracted watermark images from Airplane images under various attacks in visual observations, while tables III to V contain the NC values of watermark images from host images under various attacks. These figures demonstrate that the extracted watermark images are fully extracted and resemble the original watermark images. These tables and figures demonstrate that the presented watermarking technique performs better in terms of both invisibility and resilience to attacks. The presented watermarking technique is contrasted with the existing method, which made use of the identical host images and the identical watermark image (watermark_3) for more investigation.

TABLE III. THE EXTRACTED WATERMARK'S NC VALUES WITH WATERMARK_1 UNDER VARIOUS ATTACKS

Attack	Airplane	Sailboat	Peppers	Baboon	Lena
Crop.	1.000	0.999	1.000	1.000	1.000
Scaling	0.997	0.994	0.994	0.996	0.992
Poisson	1.000	0.999	0.999	0.992	0.999
Blurring	0.997	0.994	0.993	0.996	0.993
Gamma	1.000	0.999	1.000	1.000	1.000
Sharp.	0.997	0.990	0.988	0.983	0.996
Flip.	1.000	0.999	1.000	1.000	1.000
JPEG	0.866	0.949	0.938	0.974	0.884
Median	0.957	0.949	0.948	0.926	0.955

A comparison between the presented watermarking technique and this existing method is shown in Table VI [32] and a visual comparison is shown figure 11. This table shows that the presented watermarking technique performs better than the existing scheme in terms of invisibility.

TABLE IV. THE EXTRACTED WATERMARK'S NC VALUES WITH WATERMARK_2 UNDER VARIOUS ATTACKS

Attack	Airplane	Sailboat	Peppers	Baboon	Lena
Crop.	1.000	1.000	1.000	0.999	1.000
Scaling	0.990	0.993	0.990	0.991	0.991
Poisson	0.998	0.999	0.998	0.975	1.000
Blurring	0.992	0.994	0.990	0.992	0.992
Gamma	1.000	1.000	1.000	0.999	1.000
Sharp.	0.997	0.989	0.989	0.957	0.995
Flip.	1.000	1.000	1.000	0.999	1.000
JPEG	0.893	0.945	0.927	0.969	0.906
Median	0.924	0.911	0.909	0.903	0.919

TABLE V. THE EXTRACTED WATERMARK'S NC VALUES WITH WATERMARK_3 UNDER VARIOUS ATTACKS

Attack	Airplane	Sailboat	Peppers	Baboon	Lena
Crop.	1.000	0.998	1.000	0.999	1.000
Scaling	0.994	0.993	0.994	0.992	0.993
Poisson	1.000	0.997	0.998	0.990	0.999
Blurring	0.994	0.993	0.994	0.994	0.994
Gamma	1.000	0.998	1.000	0.999	1.000
Sharp.	0.996	0.988	0.987	0.980	0.996
Flip.	1.000	0.998	1.000	0.999	1.000
JPEG	0.852	0.940	0.932	0.968	0.874
Median	0.945	0.935	0.943	0.916	0.959

TABLE VI. THE COMPARISON OF THE PROPOSED SCHEME OF WATERMARK 2 WITH THE EXISTING SCHEME

Image	Scheme	PSNR
Baboon	[32]	47.070
	Proposed	47.389
Peppers	[32]	47.070
	Proposed	51.623
Lena	[32]	47.070
	Proposed	54.687

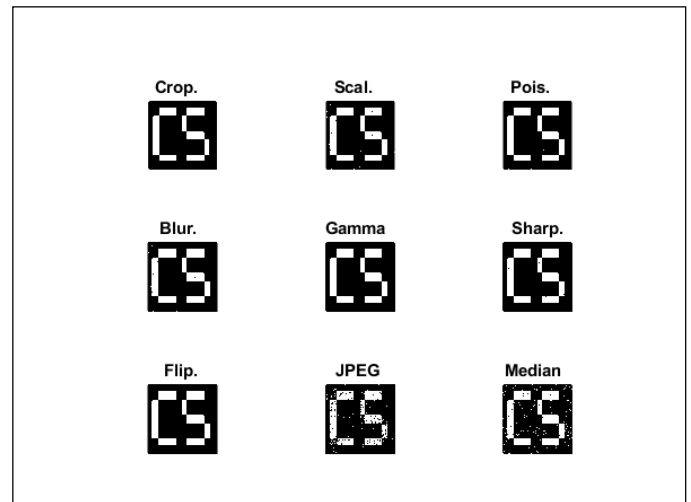


Fig. 9. The extracted watermark_2 from the Airplane image with several attacks.

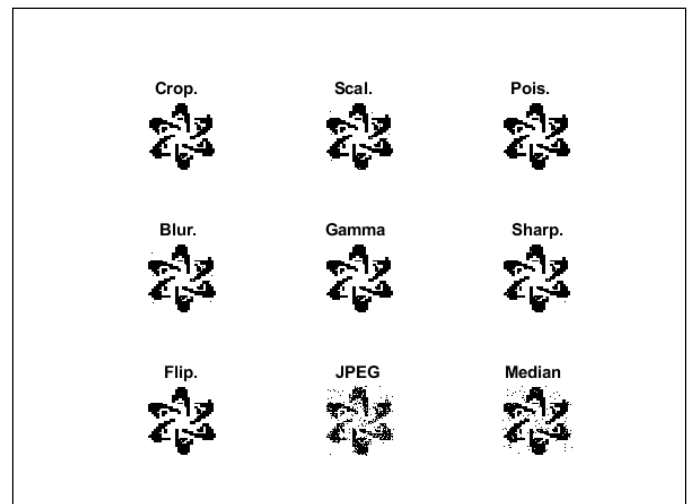


Fig. 10. The extracted watermark_3 from the Airplane image with several attacks

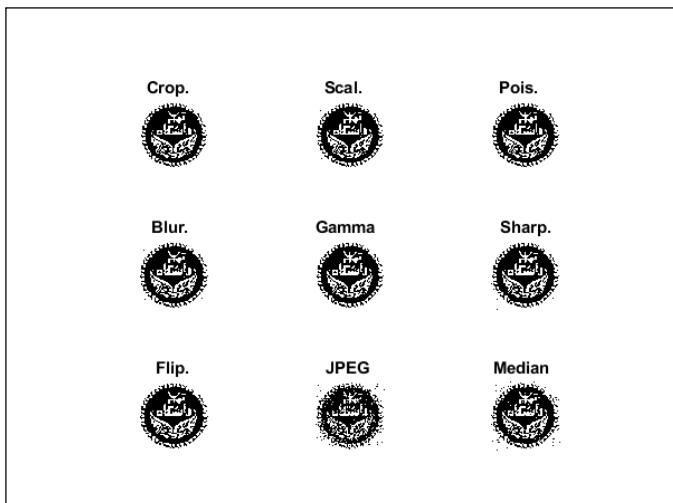


Fig. 8. The extracted watermark_1 from the Airplane image with several attacks.

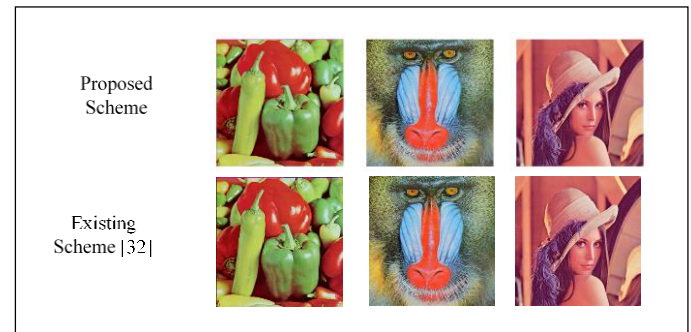


Fig. 11. The visual comparison of the proposed scheme of watermark 3 with the existing scheme under no_attack.

V. CONCLUSION

This work presents a blind color image watermarking scheme for copyright protection that relies on entropy analysis, lifting wavelet transform, QR factorization and discrete cosine transform. There are three primary features of this study: (1) To increase invisibility and robustness to attacks, DCT, LWT, and QR factorization are applied. (2) To

improve the security of the presented scheme, a pseudo-random sequence is employed. (3) The entropy analysis is utilized to achieve a better trade-off between robustness and imperceptibility. The experimental findings demonstrate the presented algorithm's high security, good imperceptibility, and strong robustness to various attacks. Future research will concentrate on integrating color watermark images into host color images.

REFERENCES

- [1] K. M. Hosny, M. M. Darwish, and M. M. Fouda, "Robust color images watermarking using new fractional-order exponent moments," *IEEE Access*, vol. 9, pp. 47425-47435, 2021.
- [2] R. Sinhal, I. A. Ansari, and C. W. Ahn, "Blind image watermarking for localization and restoration of color images," *IEEE Access*, vol. 8, pp. 200157-200169, 2020.
- [3] A. K. Sahu, "A logistic map based blind and fragile watermarking for tamper detection and localization in images," *Journal of Ambient Intelligence and Humanized Computing*, vol. 13, no. 8, pp. 3869-3881, 2022.
- [4] J. Wang, W. B. Wan, X. X. Li, J. De Sun, and H. X. J. E. S. w. A. Zhang, "Color image watermarking based on orientation diversity and color complexity," vol. 140, p. 112868, 2020.
- [5] O. Abodena, "An Optimized Image Watermarking Technique Based on LU Factorization and Entropy Analysis," *AL-JAMEAI*, vol. 39, no. 2, pp. 21-38, 2024.
- [6] D. Liu, Q. Su, Z. Yuan, and X. J. S. P. I. C. Zhang, "A blind color digital image watermarking method based on image correction and eigenvalue decomposition," vol. 95, p. 116292, 2021.
- [7] O. Abodena and M. Agoyi, "Colour image blind watermarking scheme based on fast walsh hadamard transform and hessenberg decomposition," *Studies in Informatics and Control*, vol. 27, no. 3, pp. 339-348, 2018.
- [8] A. Zear and P. K. Singh, "Secure and robust color image dual watermarking based on LWT-DCT-SVD," *Multimedia Tools and Applications*, vol. 81, no. 19, pp. 26721-26738, 2022.
- [9] R. Chu, S. Zhang, J. Mou, and X. Gao, "A zero-watermarking for color image based on LWT-SVD and chaotic system," *Multimedia Tools and Applications*, vol. 82, no. 22, pp. 34565-34588, 2023.
- [10] O. Abodena, "A Robust Blind Grayscale Image Watermarking Technique Based on Schur Decomposition and Entropy Analysis," *University Gharyan Journal*, vol. 28, no. 2, pp. 471-493, 2023.
- [11] F. Nejati, H. Sajedi, and A. Zohourian, "Fragile watermarking based on QR decomposition and Fourier transform," *Wireless Personal Communications*, vol. 122, no. 1, pp. 211-227, 2022.
- [12] O. Abodena, M. Agoyi, and E. Celebi, "Hybrid technique for robust image watermarking using discrete time fourier transform," in *2017 25th Signal Processing and Communications Applications Conference (SIU)*, 2017: IEEE, pp. 1-4.
- [13] C. Qu, J. Du, X. Xi, H. Tian, and J. Zhang, "A hybrid domain-based watermarking for vector maps utilizing a complementary advantage of discrete fourier transform and singular value decomposition," *Computers & Geosciences*, vol. 183, p. 105515, 2024.
- [14] O. Abodena, "Robust and high-capacity audio watermarking based on chirp z-transform," in *2021 29th Signal processing and communications applications conference (SIU)*, 2021: IEEE, pp. 1-4.
- [15] B. Singh and M. Sharma, "Watermarking technique for document images using discrete curvelet transform and discrete cosine transform," *Multimedia Tools and Applications*, pp. 1-25, 2024.
- [16] E. Gul, "A blind robust color image watermarking method based on discrete wavelet transform and discrete cosine transform using grayscale watermark image," *Concurrency and Computation: Practice and Experience*, vol. 34, no. 22, p. e6884, 2022.
- [17] O. Abodena and A. Alashtir, "High Hiding Capacity Audio Watermarking Method Based on Discrete Cosine Transform," *Internation Journal Of Advance Research And Innovative Ideas In Education*, vol. 7, pp. 677-684, 2021.
- [18] A. Tiwari and V. K. Srivastava, "Image watermarking techniques based on Schur decomposition and various image invariant moments: a review," *Multimedia Tools and Applications*, vol. 83, no. 6, pp. 16447-16483, 2024.
- [19] S. Y. Altay and G. Ulutas, "Biometric watermarking schemes based on QR decomposition and Schur decomposition in the RIDWT domain," *Signal, Image and Video Processing*, vol. 18, no. 3, pp. 2783-2798, 2024.
- [20] N. Phuong Thi and T. Ta Minh, "A new block selection strategy from LU decomposition domain for robust image watermarking," *Multimedia Tools and Applications*, vol. 83, no. 7, pp. 19301-19325, 2024.
- [21] D.-O. Muñoz-Ramírez, B.-P. García-Salgado, V. Ponomaryov, R. Reyes-Reyes, S. Sadovnychiy, and C. Cruz-Ramos, "A color image watermarking framework for copyright protection of stereo images based on binocular just noticeable difference and LU decomposition," *Multimedia Tools and Applications*, vol. 80, pp. 13707-13734, 2021.
- [22] Y. Chen, Z.-G. Jia, Y. Peng, Y.-X. Peng, and D. Zhang, "A new structure-preserving quaternion QR decomposition method for color image blind watermarking," *Signal Processing*, vol. 185, p. 108088, 2021.
- [23] P. T. Nha, T. M. Thanh, and N. T. Phong, "Consideration of a robust watermarking algorithm for color image using improved QR decomposition," *Soft Computing*, vol. 26, no. 11, pp. 5069-5093, 2022.
- [24] Y. Luo *et al.*, "A multi-scale image watermarking based on integer wavelet transform and singular value decomposition," *Expert Systems with Applications*, vol. 168, p. 114272, 2021.
- [25] T. Zhu, W. Qu, and W. Cao, "An optimized image watermarking algorithm based on SVD and IWT," *The Journal of Supercomputing*, vol. 78, no. 1, pp. 222-237, 2022.
- [26] K. Fujinoki and K. Ashizawa, "Directional lifting wavelet transform for image edge analysis," *Signal Processing*, vol. 216, p. 109188, 2024.
- [27] B. Bao and Y. Wang, "A robust blind color watermarking algorithm based on the Radon-DCT transform," *Multimedia Tools and Applications*, pp. 1-20, 2024.
- [28] C. Lourenco and E. Moreno-Centeno, "Exact QR factorizations of rectangular matrices," *Optimization Letters*, vol. 18, no. 3, pp. 681-695, 2024.
- [29] S. Kumar and B. K. Singh, "Entropy based spatial domain image watermarking and its performance analysis," *Multimedia Tools and Applications*, vol. 80, no. 6, pp. 9315-9331, 2021.
- [30] A. G. Weber, "The USC-SIPI image database: Version 5," <http://sipi.usc.edu/database/>, 2006.
- [31] O. Abodena, "A robust blind watermarking scheme based on lifting wavelet transform and hessenberg decomposition," *Journal of Pure & Applied Sciences*, vol. 21, no. 2, pp. 48-54, 2022.
- [32] M. Li, X. Yuan, H. Chen, and J. Li, "Quaternion discrete fourier transform-based color image watermarking method using quaternion QR decomposition," *IEEE Access*, vol. 8, pp. 72308-72315, 2020.